2010 Fourth International Conference on Sensor Technologies and Applications

Stacked photo-sensing devices based on SiC alloys

A non-pixelled architecture for imagers and demultiplexing devices

M. Vieira[1,2] , P. Louro[1,2], M. Fernandes[1,2], A. Fantoni, M. A. Vieira[1,2], J. Costa[1,2],
[1]Electronics Telecommunications and Computer Dept, ISEL, Lisbon, Portugal.
[2]CTS-FCT-UNL, Quinta da Torre, 2829-516, Caparica, Portugal,
mv@isel.ipl.pt

***Abstract*— In this review paper different designs based on stacked p-i'-n-p-i-n heterojunctions are presented and compared with the single p-i-n sensing structures. The imagers utilise self- field induced depletion layers for light detection and a modulated laser beam for sequential readout. The effect of the sensing element structure, cell configurations (single or tandem), and light source properties (intensity and wavelength) are correlated with the sensor output characteristics (light-to-dark sensivity, spatial resolution, linearity and S/N ratio). The readout frequency is optimized showing that scans speeds up to 10^4 lines per second can be achieved without degradation in the resolution. Multilayered p-i'-n-p-i-n heterostructures can also be used as wavelength-division multiplexing /demultiplexing devices in the visible range. Here the sensor element faces the modulated light from different input colour channels, each one with a specific wavelength and bit rate. By reading out the photocurrent at appropriated applied bias, the information is multiplexed or demultiplexed and can be transmitted or recovered again. Electrical models are present to support the sensing methodologies.**

Keywords-optical sensors; wavelength division multiplexing-demultiplexing ; electrical simulation;optical communications.

I. INTRODUCTION

Whether we hope to view images or count photons, we use devices that work by absorbing photons and turning them into information. With the advent of computers and digital image processing, electronic image sensors have become indispensable tools. Three forces direct the evolution: Advances in technology determine what is possible, algorithms determine what is practical, and applications determine what is desirable. If we wanted to generalize about areas in which detectors and imaging technology can improve, we could talk about collecting information more quickly and efficiently, at more wavelengths, with more compact and user-friendly devices or interfaces. Any conventional solid state imaging device consists of an array of sensing elements combined with some form of transport mechanism to deliver the sensor output signal to the periphery of the device [1, 2, 3].

Amorphous silicon-carbon (a-SiC:H) is a material that exhibits excellent photosensitive properties. This feature together with the strong dependence of the maximum spectral response with the applied bias has been intensively used for the development of colour devices [4 , 5, 6]. In our group efforts have been devoted towards the development of a new kind of colour sensor. Large area hydrogenated amorphous silicon single and stacked p-i-n structures with low conductivity doped layers were proposed as colour Laser Scanned Photodiode (LSP) image sensors [7, 8, 9]. These sensors are different from the other electrically scanned image sensors as they are based on only one sensing element with an opto-mechanical readout system. No pixel architecture is needed. The advantages of this approach are quite obvious like the feasibility of large area deposition and on different substrate materials (e.g., glass, polymer foil, etc.), the simplicity of the device and associated electronics, high resolution, uniformity of measurement along the sensor and the cost/simplicity of the detector. The design allows a continuous sensor without the need for pixel-level patterning, and so can take advantage of the amorphous silicon technology. It can also be integrated vertically, i. e. on top of a read-out electronic, which facilitates low cost large area detection systems where the signal processing can be performed by an ASIC chip underneath.

The current need for communication demands the transmission of huge amounts of information. To increase the capacity of transmission and allow bidirectional communication over one strand fiber, wavelength-division multipexing (WDM) is used [10]. Although the WDM systems are well known for infrared telecommunication systems, they must be completely renewed for the different windows transmission over Polymer Optical Fibers (POF) in the visible spectrum.

In this review paper different designs based on stacked p-i'-n-p-i-n heterojunctions are presented and compared with the single p-i-n sensing structures.

II. EXPERIMENTAL DETAISL

A. Device configuration and preparation

Voltage controlled devices, were produced in different architectures and tested for a proper fine tuning of the visible spectrum. The tandem devices (#2a, b), have a p-i'-n/p-i-n configuration with the absorber of the back diode (i-) based on a-Si:H and the front intrinsic layers based on a-SiC:H (i'-). To test the efficiency of the internal n-p junction, a third transparent contact was deposited in-between (#2b).

978-0-7695-4096-2/10 $26.00 © 2010 IEEE
DOI 10.1109/SENSORCOMM.2010.16

In all the devices the thickness (200nm) and the optical gap (2.1 eV) of the a-SiC:H intrinsic layer (i'-) are optimized for blue collection and red transmittance and the thickness (1000 nm) of a-Si:H one (i-) adjusted to achieve full absorption in the green and high collection in the red spectral range. As a result, both front and back diodes act as optical filters confining, respectively, the blue and the red optical carriers, while the green ones are absorbed across both [11].

The deposition conditions of the i- (based on a-Si:H) and i'- (based on a-SiC:H) were kept constant in all the devices. The i- and i' layers present good optoelectronic properties with conductivities between 10^{-11} and $10^{-9}\Omega^{-1}$ cm^{-1} and photosensitivity higher than 10^4 under AM1.5 illumination (100 mW/ cm^2). Transparent contacts have been deposited on front and back surfaces to allow the light to enter and leave from both sides. The different architectures are displayed in Figure 1. In the single configuration (#1), the device is a p-i-n photodiode with intrinsic layers (i-) based on a-SiH.

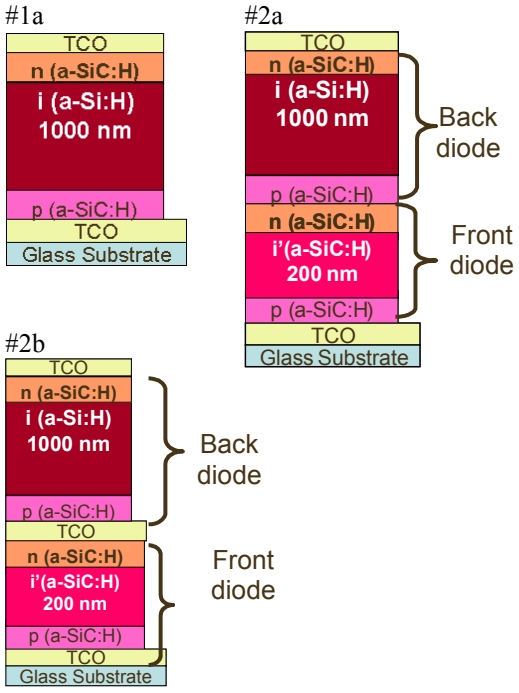

Figure 1. WDM device configuration.

In order to produce highly resistive (>$10^7\Omega$cm) and wide band gap doped layers (≅2.1 eV), which is of crucial importance for device operation, during the deposition process, low doping levels were used and methane was added [12]. The back contact defines the active area of the sensor (4×4 cm^2)**.**The front and back contacts are based on ZnO:Al or ITO and have an average transmission around 80% from 425 nm to 700 nm and a resistivity around $9x10^{-4}$ Ωcm.

B. Optoelectronic Characterization

The characterisation of the devices was performed through the analysis of the photocurrent dependence on the applied voltage and spectral response under different optical and electrical bias conditions. The responsivity was obtained by normalizing the photocurrent to the incident flux. To suppress the *dc* components all the measurements were performed using the lock-in technique.

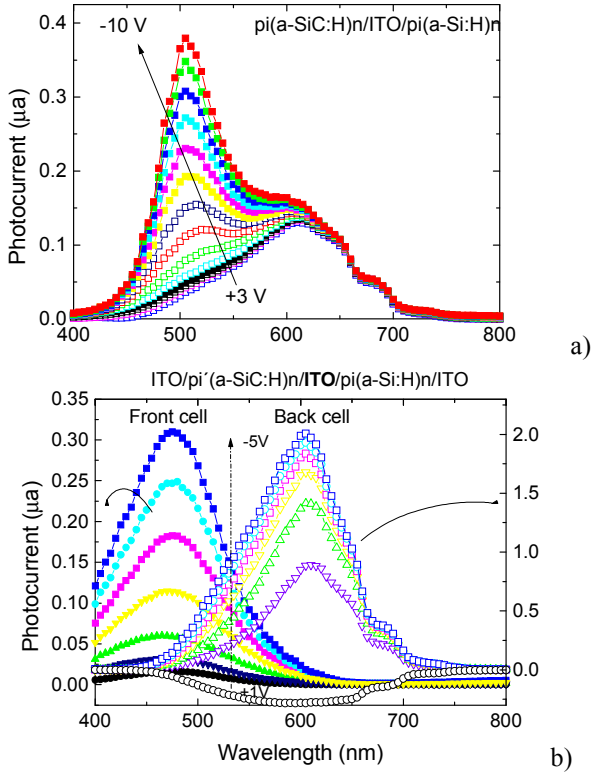

Figure 2. a) p-i'-n-p-i-n spectral photocurrent under different applied voltages b)Front, p-i' (a-SiC:H)-n, and back, p-i (a-Si:H)-n: a) spectral photocurrent under different applied bias.

Figure 2a displays the spectral photocurrent of the sensor #2b under different applied bias (+3V<V<-10V), the internal transparent contact was kept floating in all measurements. In Figure 2b the spectral photocurrent, under different electrical bias is displayed for the front, p-i' (a-SiC:H)-n, and the back p-i (a-Si:H)-n, photodiodes.

Results confirm that the front and back photodiodes act, separately, as optical filters. The front diode, based on a-SiC:H heterostructure, cuts the wavelengths higher than 550nm while the back one, based on a-Si:H, cuts the ones lower than 500nm. Each diode, separately, presents the typical responses of single p-i-n cells with intrinsic layers based on a-SiC:H or a-Si:H materials, respectively. Since the current across the device has to remain the same, in the stacked configuration, is clearly observed the influence of both front and back diodes modulated by its serial connection through the internal n-p junction.

C. Ligth-to-dark sensitivity

To improve the light-to-dark sensitivity in sensor #1, doped layer resistivity and optical gap were optimized. In Figure 3 the sensitivity as a function of the wavelength is

displayed under no optical bias (Φ_L=0) and under uniform illumination (530 nm, 2 mWcm^{-2}), respectively. Three samples were deposited keeping constant the deposition conditions for all i-layers, while they varied in the doped layers by adding methane during the deposition process. All the layers on sample #1 are based a-Si:H; (homostructure), while the p-layer in #1b and the p- and n-layers in #1 are based on a-SiC:H alloy (heterostructures).

Data reveal that the sensitivity, when wide band gap doped layers are used, is lower and decreases significantly with the optical bias. Under steady state irradiation the band misalignment reduces the electrical field in the bulk and increases the recombination at the interfaces decreasing the carrier collection.

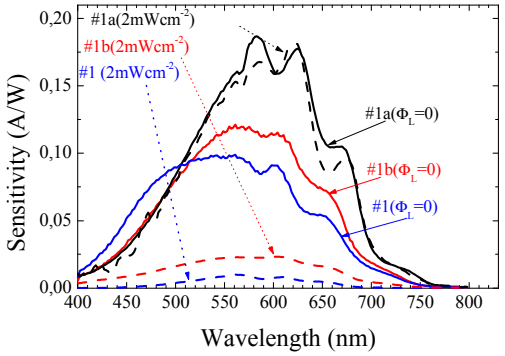

Figure 3. Spectral sensitivity with (dash) and without (solid) applied optical bias.

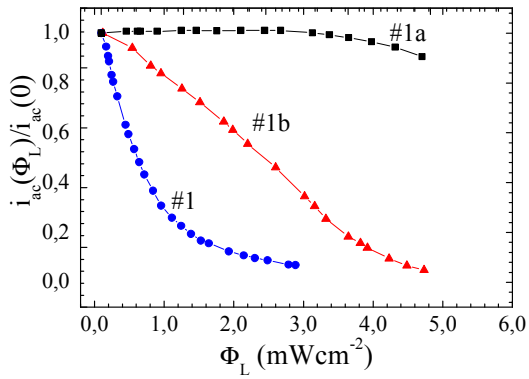

Figure 4. $i_{ac}(\Phi_L)/i_{ac}(0)$ ratio dependence with Φ_L

In Figure 4 we plot the light to dark sensitivity as a function of the applied optical bias, Φ_L. Results show that also the light-to-dark ratio depends strongly on the material of the doped layers. In the heterostructures the responsivity for low fluxes is high, while in the homostructure only a small signal could be detected in the flux range analyzed. When the sensor has both doped layers based on a-SiC:H layers (#1) the signal ratio steeply decreases. If only one layer is based on a-SiC:H (#1b) the signal ratio also decrease but in a slower rate. Finally, in the homostructure (#1a) the sensor remains "blind" to the optical bias and only at higher light fluxes the signal ratio gently decreases. This light bias dependence enables different application of the device depending on the readout technique. If a light scan is used to readout the generated carriers it can recognize a colour pattern projected on it. If the photocurrent generated by different monochromatic pulsed channels or their combination is readout the information is multiplexed or demultiplexed and can be transmitted, tuned or recovered again.

D. Optical amplification

Three monochromatic pulsed lights (input channels): red (R: 626 nm), green (G: 524 nm) and blue (B: 470nm) illuminated separately device #2a. Steady state red, green and blue optical bias was superimposed separately and the photocurrent generated measured at -8V and +1 V. In Figure 5 the signal is displayed for each monochromatic input channels.

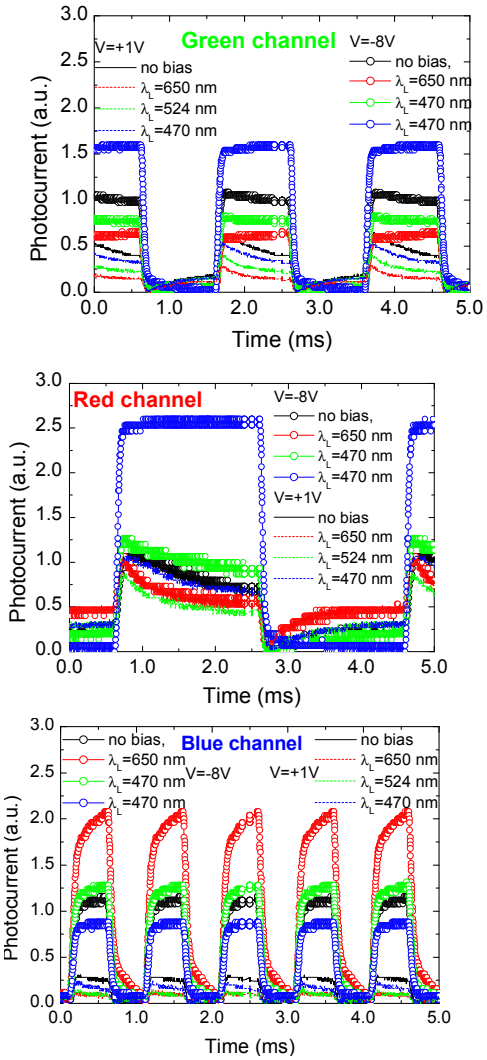

Figure 5. Input red (a) green (b) and blue (c) signals under negative and positive bias without and with red, green and blue steady state optical bias.

Results show that blue steady state optical bias amplifies the red channel and the red light amplifies the blue channel.

When an optical bias is applied it mainly enhances the field distribution within the less photo excited sub-cell: the back under blue irradiation and the front under red steady bias. So, the reinforcement of the electric field under blue irradiation and negative bias increases the collection of the carriers generated by the red channel and decrease the blue one. Under red optical bias an opposite behaviour is observed. The green bias absorption is balanced in both front and back cells. So, the green channel collection is reduced while the red and blue collections are almost insensitive to the green irradiation. This effect can be used either to amplifier the red or blue channels or to tune the green one since the others remain almost constant.

III. READOUT TECHNIQUES

A. *Laser scanned photodiode (LSP) technique*

The image readout process relies on the same principle for both single and stacked structures. An optical image is projected onto the active surface from the glass side and is scanned by sequentially detecting scene information at discrete XY coordinates. In the single (#1) heterostructure the image and the scanner are incident on the same side while in double one (#2a) they are opposite. This last approach simplifies the optical system since image and scanner have different optical paths. A 633 nm low power solid-state laser was used as scanner. The beam deflection is controlled by a two axis deflection system capable of high speed scan.

The read-out of the injected carriers is achieved by measuring, under appropriated applied voltages, the *ac* component of the current, i_{ac}, which depends on the intensities of both the image and the scanner. This component can be analytically described by the equation 1,

$$i_{ac} = R(\Phi_L)\cdot\Phi_S\cdot\frac{\pi d^2}{4} \quad (1)$$

$$S/N = \frac{i_{ac}^2}{(4kT/R_0 + 2q.I_{DC})\Delta f} \quad (2)$$

where $R(\Phi_L)$ is the small signal responsivity at a given illumination Φ_L, Φ_S is the average power density of the scanner beam and d its diameter. The signal-to-noise power ratio (S/N) depends on both components of the photocurrent (i_{ac} and I_{DC}) and is given by equation 2, where Δf is the bandwidth and R_0 the sensor resistance at zero voltage bias.

The current is amplified by a current to voltage converter with selectable gain and converted to digital format by a signal acquisition card installed on a computer. Two additional photodiodes provide the synchronization signals for scanner position information, necessary for the image restoration process. The data is stored as a matrix of photocurrent values which provide information about local illumination conditions on each position of the active area of the device. Further processing algorithms like fixed pattern noise suppression are performed by software.

B. *LSP image sensor (single vs double configurations)*

In order to analyze the behaviour of the single configuration under different voltages a pattern composed by dark and illuminated regions was projected on device #1.

In Figure 6 are represented the scans of the image under forward, reverse and zero bias voltage. The image brightness ($2\mu Wcm^{-2}$), scanner intensity (two order of magnitude lower) and spot diameter (50 µm) were kept constant. Results show that under reverse bias the image sensitivity and the dynamic range are higher than in short circuit or forward bias. In reverse mode a dynamic rate of two orders of magnitude with a sensitivity of 6 mA/W and a responsivity of 17 μWcm^{-2} were achieved. As a possible applications in Fig. 6b we also display a grayscale photo and a fingerprint representation acquired under short circuit and Φ_L =10 μWcm^{-2}.

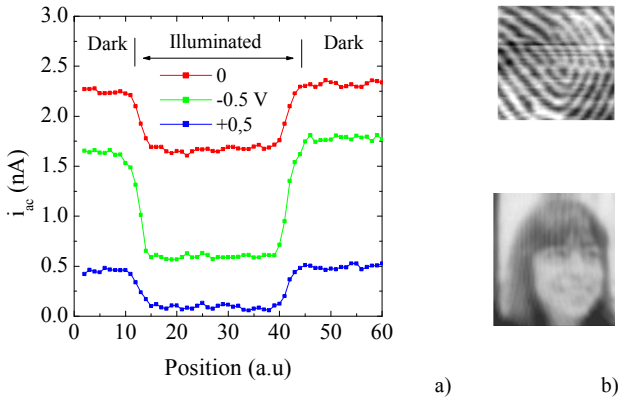

Figure 6. The ac photocurrent for one dimension scan under forward, reverse and zero bias. b) grayscale photo and a fingerprint representations

No image processing algorithms were used. This image presents a good contrast and a resolution around 30 µm showing the potentiality of these devices for biometric applications.

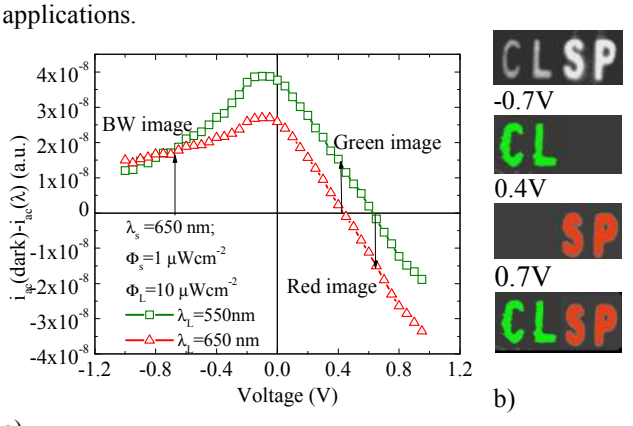

Figure 7. a) Image intensity as a function of the electrical bias under different optical bias. b) A picture image of the sensor acronym CLSP with green "CL" and red "SP".

In Figure 7 the image output signal [13] defined as the difference between the ac component of the photocurrent in

dark (Φ_L=0) and under illumination (λ_s=550 nm, 650 nm and Φ_L=10 μWcm^{-2}) is displayed as a function of the electrical bias. Data show that at -0.7 V, the image intensity for the red or the green image presents the same magnitude and signal. No colour information can be extracted at this voltage, which leads to a black and white image. In this mode the brightness of the image is proportional to the output signal (i_{ac}), which gives to the sensor the ability of acquiring monochrome gray level images. Colour information can only be obtained under forward bias. By tuning the voltage to 0.4 V the red signal is suppressed allowing green recognition. The red information is obtained at 0.7 V, where the green signal goes down to zero. Combining the signal information at these voltages (-0.7 V; 0.4 V, 0.7 V) enables the reconstruction of the colour image without the need of the usual colour filters. A picture image of the sensor acronym CLSP (Colour Laser Scanned Photodiode) with green "CL" and red "SP" was projected onto the sensor. The result is shown in Fig. 7b at V=-0.7V, V=0.4 V and V=0.7 V. The full colour image in was obtained by combining the information.

C. *Optically addressed image and colour sensor*

In #2a configuration full colour detection is attempt based on spatially separated absorption of the red, green and blue photons (Figure 2).

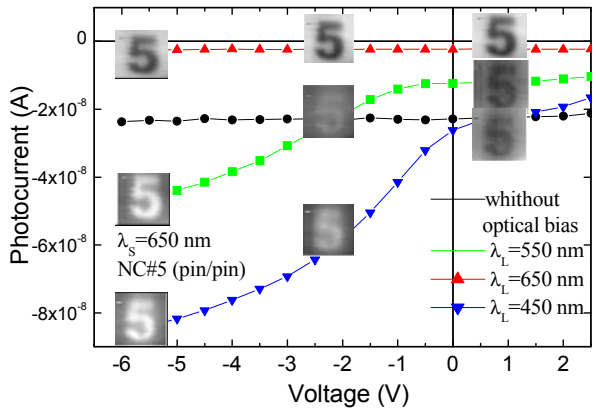

Figure 8. Photocurrent as a function of the applied bias for sensor #2a in dark and under blue, green and red irradiation. The inserts show, at the acquired applied voltages, the images from the same RGB picture (5).

In Figure 8 the photocurrents generated by the scanner under different steady-state illumination conditions (Φ_L=200 μWcm^{-2}, λ_L=650 nm; 550 nm; 450nm) are displayed. The images, defined as the difference between the photocurrents with and without optical bias, are shown as inserts, at the acquired applied voltages. Here the same green, red and blue pictures (**5**) were projected, one by one, onto the front diode and acquired through the back one with a moving red scanner. The line scan frequency was close to 1 kHz and no algorithms where used during the image restoration process. For readout time of 1 ms the frame time, for a 50 lines image, is around 50 ms. Results show that under red irradiation or in dark (without optical bias) the photocurrent generated by a red scanner is independent on the applied voltage. Under blue/green irradiation it decreases as the applied voltage changes from reverse to forward being higher under blue than under green irradiation. As expected from Figure 5 the main difference occurs in the green spectral range. It is interesting to notice that around -2 V the collection with or without green image are the same, leading to the rejection of the green image signal. So, by tuning the voltage to -2 V the red and blue signal are high and opposite in sign and the green signal is suppressed allowing blue and red colour recognitions. The green information is obtained under slight forward bias (+1 V), where the blue signal goes down to zero and the red remains constant. Combining the information obtained at three applied voltages a RGB colour image can be acquired without the need of the usual colour filters or pixel architecture.

By sampling the absorption region at different applied bias voltages it was possible to extract separately the RGB integrated information with a good rejection ratio. Readout of 1000 lines per second was achieved allowing continuous and fast image sensing, and colour recognition.

IV. Wavelength-Division (De)Multiplexing Technique

Monochromatic pulsed beams together or one single polychromatic beam (mixture of different wavelength) impinge in the device and are absorbed, accordingly to their wavelength (Figures 2 and 5). By reading out, under appropriated electrical bias conditions, the photocurrent generated by the incoming photons, the input information is electrically multiplexed or demultiplexed.

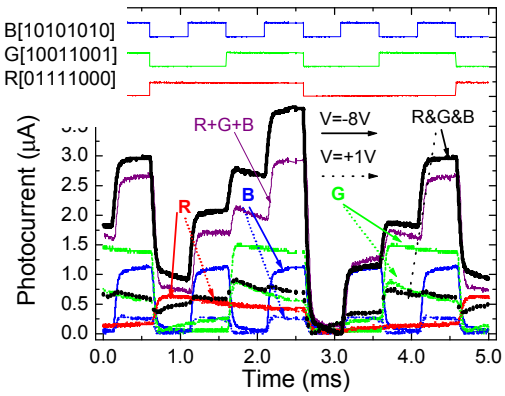

Figure 9. Single (R, G and B) and combined (R&G&B) signals under -8V (solid arrows) and +1V (dotted arrows).

In the multiplexing mode the device faces the modulated light incoming together from the fibers (monochromatic input channels). The combined effect of the input signals is converted to an electrical signal, via the device, keeping the input information (wavelength, intensity and modulation frequency). In the demultiplexing mode a polychromatic modulated light beam is projected onto the device and the readout performed by shifting between forward and reverse bias. Figure 9 displays the input and multiplexed signals under negative (-8V) and positive (+1V) electrical bias. As expected from Figures 2, 5 and 8, the input red signal

remains constant while the blue and the green ones decrease as the voltage changes from negative to positive.

The output multiplexed signal, obtained with the combination of the three optical sources, depends on both the applied voltage and on the ON-OFF state of each input optical channel. Under negative bias, the multiplexed signal presents eight separate levels. The highest level appears when all the channels are ON and the lowest if they are OFF. Furthermore, the levels ascribed to the mixture of three or two input channels are higher than the ones due to the presence of only one (R, G, B).

Optical nonlinearity was detected; the sum of the input channels (R+B+G) is lower than the correspondent multiplexed signals (R&G&B). This optical amplification, mainly on the ON-ON states, suggests capacitive charging currents due to the time-varying nature of the incident lights. Under positive bias the levels were reduced to one half since the blue component of the combined spectra falls into the dark level, the red remains constant and the green component decreases (Figures 3, 5 and 8).

To recover the transmitted information (8 bit per wavelength channel) the multiplexed signal, during a complete cycle, was divided into eight time slots, each corresponding to one bit where the independent optical signals can be ON (1)or OFF (0). Under positive bias, the device has no sensitivity to the blue channel, so the red and green transmitted information are tuned and identified. The highest level corresponds to both channels ON (R=1, G=1), and the lowest to the OFF-OFF stage (R=0; G=0). The two levels in-between are related with the presence of only one channel ON, the red (R=1, G=0) or the green (R=0, G=1). To distinguish between these two situations and to decode the blue channel, the correspondent sub-levels, under reverse bias, have to be analyzed. The highest increase at -8V corresponds to the blue channel ON (B=1), the lowest to the ON stage of the red channel (R=1) and the intermediate one to the ON stage of the green (G=1). Using this simple key algorithm the independent red, green and blue bit sequences were decoded as: R[01111000], G[10011001] and B[10101010], as shown on the top of Figure 10, which are in agreement with the signals acquired for the independent channels.

V. TWO-TRANSISTOR MODEL AND VALIDATION

The silicon-carbon pi'npin device can be considered as a monolithic double pin photodiode structure with two red and blue optical connections for light triggering. Based on the experimental results and device configuration an electrical model was developed [14]. Operation is explained in terms of the compound connected phototransistor equivalent model displayed as an insert in Figure 10.

When the pi'npin device is reverse-biased, the base emitter junction of both transistors are inversely polarized and conceived as phototransistors, taking, so, advantage of the amplifier action of neighboring collector junctions which are polarized directly. This results in a charging current gain proportional to the ratio between both collector currents (C_1/C_2). Under positive bias the internal junction becomes always reverse-biased. If not triggered ON it is nonconducting, when turned ON by light it conducts like a photodiode, for one polarity of current.

In Figure 10 the simulated multiplexed (symbols), current sources (dash lines) and the experimental (solid lines) signals are compared under: a) positive (R_1=10MΩ; +1V) and negative (R_1=1KΩ; -8V) dc bias. Good agreement between experimental and simulated data was observed. The expected levels, under reversed bias, and their reduction under forward bias are clearly seen (Figure 9). Under negative bias (low R_1), the device behaves like a transmission system able to store and transport all the minority carriers generated by the current pulses, through the capacitors C_1 and C_2. Under positive bias (high R_1) the device remains in its non conducting state unless a light pulse is applied to the base of Q_2. This pulse causes Q_2 to conduct because the reversed biased n-p internal junction behaves like a capacitor inducing a charging current across both collector junctions.

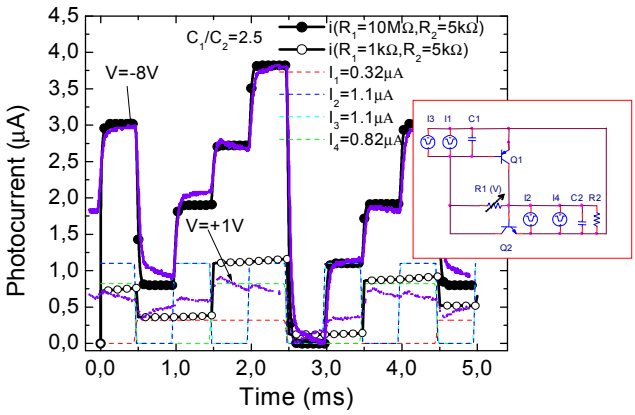

Figure 10. Simulated multiplexed (symbols), current sources (dash lines) and experimental (solid lines) signals under: a) positive (R1=10MΩ; +1V) and negative (R1=1KΩ; -8V) dc bias. Insert : ac circuit representation.

Under forward bias (high R_1) the device remains in its non conducting state unless a light pulse (I_2 or I_2+I_4) is applied to the base of Q_2. This pulse causes Q_2 to conduct because the reversed biased n-p internal junction behaves like a capacitor inducing a charging current (I_2+I_4) across both collector junctions. The collector of the conducting transistor pulls low, moving the Q_1 base toward its collector voltage, which causes Q_1 to conduct. The collector of the conducting Q_1 pulls high, moving the Q_2 base in the direction of its collector. This positive feedback (regeneration) reinforces the Q_2 already conducting state and a current I_2+I_4 will flow on the external circuit.

This two transistor model also explains the use of the same configuration in the Laser Scanned Photodiode (LSP) image and colour sensor. Each successive diode acts as a filter for the diode below it (Figures 1 and 2) shifting the spectrum of absorbed light in successive layers. By deconvolving the response of each photodetector, using a moving red pulse (scanner; I_2), dark, red, green, and blue pattern can be reconstructed (Figure 8) and a color image acquired.Experimental results have shown that the deep penetration of the red photons exclusively into the back

diode, and the transparency of the front diode to them push the electrical field up in the front diode (self-reverse effect) and down into the back one (self-forward effect) [15]. The shallow penetration of the blue photons exclusively into the front diode changes the electrical fields in an opposite way resulting in a collection that depends on the applied voltage. In the green range both reverse and forward self bias effects coexists. To cancel the effect of the green illumination a reverse bias is needed.

For the colour image sensor electrical model only the red channel is used (Figure 11a, $I_2 \neq 0$, $I_1=I_3=I_4=0$). As explained before (Figures 10 and 11), without optical bias (dark pattern) and during the red pulse, only the minority carriers generated at the base of Q_2 by the scanner (I_2 ON), flow across the circuit either in reverse or forward bias.

Under red bias (red pattern) the emitter-base junction of Q_2 becomes forward bias, I_2 decreases and the collection is reduced (Figures 5a and 8). Under blue (blue pattern) and green (green pattern) irradiations the signal depends on the applied voltage and so, on R_1 resistor. Under negative bias (low R_1) and blue pattern, the charge transferred from C_1 to C_2 due to the presence of the blue optical bias, reaches the output terminal as capacitive charging currents. An optical amplification is observed due to the amplifier action of adjacent collector junctions which are always polarized directly (Figure 5a). Under forward bias (+1V) the device remains in its non conducting state, unless the scanner pulse (I_2) is applied to the base of Q_2 resulting a current I_2 on the external circuit and consequently to the rejection of the blue image (Figure 8). Under negative voltage the behaviour under a green pattern is blue-like while under positive bias is red-like. The balance between the green absorption into the front and back diodes determines the amount of charges stored in both capacitors. Under negative bias both the green component absorbed in the front (blue-like) and the back (red-like) diodes reaches the output terminal while for voltages at witch the internal junction n-p becomes reversed, (lowers than -2V, Figure 8), the blue-like component is blocked and the red-like reduced.

So, by using a thin a-SiC:H front absorber optimized for blue collection and red transmittance and a back a-Si:H absorber to spatially decouple the green/red absorption, the model explains why a moving red scanner (probe beam) can be used to readout RGB light patterns giving information about the radiation wavelength and the position where the photons are absorbed.

VI. CONCLUSIONS

In this review paper single and stack pin heterojunctions based on a-SiC:H alloys were analysed under different optical and electrical bias conditions and compared. Two applications, each one with its own readout technique are discussed. A theoretical model gives insight on the physics of the device.

Results show that when a pinpin device is used as colour and image sensor it uses self- field induced depletion layers for light detection and a modulated laser beam for sequential readout. By sampling, at appropriated voltages, it is possible to extract separately the RGB integrated information with good rejection ratio allowing continuous and fast colour recognition and image detection. Scans speeds up to 10^4 lines per second can be achieved without degradation in the resolution. When the same pinpin configuration is used as wavelength-division multiplexing /demultiplexing devices in the visible range the sensor element faces the modulated light from different input colour channels, each one with a specific wavelength and bit rate. By reading out the photocurrent at appropriated applied bias, the information is multiplexed or demultiplexed and can be transmitted or recovered again.

Electrical models were presented to support the sensing methodologies. Experimental and simulated results show that the tandem devices act as charge transfer systems. They filter, store and transport the photogenerated carriers, keeping its memory (colour, intensity and frequency) without adding any optical pre-amplifier or optical filter as in the standard p-i-n cells.

ACKNOWLEDGEMENTS

This work is supported by CTS-UNINOVA/FCT-MCTES.

REFERENCES

[1] J. W. Horton, R. V. Mazza, and H. Dym Proc. IEEE, 52 (1964) 1513.

[2] S. Chakrabarti, O. H. W. Siegmund, and J. Hecht, Proc. SPIE 834 (1987) 222.

[3] G. J. Michon and H. K. Burk, IEEE Solid-State Circuits Conf. Digest (New York: Lewis Winner), (1974) 26.

[4] H.K. Tsai and S.C. Lee, IEEE electron device letters, EDL-8, (1987) pp.365-367. .

[5] A. Zhu, S. Coors, B. Schneider, P. Rieve, and M. Bohm, IEEE Trans. on Electron Devices, Vol. 45, No. 7, July 1998, pp. 1393-1398.

[6] M. Mulato, F. Lemmi, J. Ho, R. Lau, J. P. Lu, and R. A. Street, J. of Appl. Phys., Vol. 90, No. 3 (2001), pp. 1589-1599.

[7] M. Vieira, M. Fernandes, J. Martins, P. Louro, R. Schwarz, and M. Schubert, IEEE Sensor Journal, 1, no.2 (August, 2001) pp. 158-167.

[8] M. Vieira, M. Fernandes, P. Louro, R. Schwarz, and M. Schubert, J. Non Cryst. Solids 299-302 (2002) pp.1245-1249.

[9] M. Vieira, A. Fantoni, M. Fernandes, P. Louro, and I. Rodrigues. Mat. Res. Soc. Symp. Proc 762@2003 A.18.13.

[10] S. Randel, A.M.J. Koonen, S.C.J. Lee, F. Breyer, M. Garcia Larrode, J. Yang, A. Ng'Oma, G.J Rijckenberg, and H.P.A. Boom.. ECOC 07 (Th 4.1.4). (pp. 1-4). Berlin, Germany, 2007.

[11] P. Louro, M. Vieira, Yu. Vygranenko, A. Fantoni, M. Fernandes, G. Lavareda, and N. Carvalho, Mat. Res. Soc. Symp. Proc., 989 (2007) A12.04.

[12] P. Louro, M. Vieira, Yu. Vygranenko, M. Fernandes, R. Schwarz, and M. Schubert, Applied Surface Science 184, 144-149 (2001).

[13] M. Vieira, P. Louro, M. Fernandes, and A. Fantoni, Sensor and Actuators A 114/2-3 (2004), pp. 219-223.

[14] M. A. Vieira, M. Vieira, M. Fernandes, A. Fantoni, P. Louro, and M. Barata, Amorphous and Polycrystalline Thin-Film Silicon Science and Technology 2009, MRS Proceedings Vo. 1153, A08-0.

[15] M. Vieira, A. Fantoni, P. Louro, M. Fernandes, R. Schwarz, G. Lavareda, and C.N. Carvalho, Vacuum, Vol. 82, Issue 12, 8 August 2008, pp: 1512-1516.